Rigid-Object Water-Entry Impact Dynamics: Finite-Element/Smoothed Particle Hydrodynamics Modeling and Experimental Validation

Ravi Challa
School of Civil and Construction Engineering,
Oregon State University,
Corvallis, OR 97331

Solomon C. Yim
Professor
Coastal and Ocean Engineering Program,
School of Civil and Construction Engineering,
Oregon State University,
Corvallis, OR 97331

V. G. Idichandy
Professor
Department of Ocean Engineering,
Indian Institute of Technology Madras,
Chennai 600036, Tamilnadu, India

C. P. Vendhan
Professor
Department of Ocean Engineering,
Indian Institute of Technology Madras,
Chennai 600036, Tamilnadu, India

A numerical study on the dynamic response of a generic rigid water-landing object (WLO) during water impact is presented in this paper. The effect of this impact is often prominent in the design phase of the re-entry project to determine the maximum force for material strength determination to ensure structural and equipment integrity, human safety and comfort. The predictive capability of the explicit finite-element (FE) arbitrary Lagrangian-Eulerian (ALE) and smoothed particle hydrodynamics (SPH) methods of a state-of-the-art nonlinear dynamic finite-element code for simulation of coupled dynamic fluid structure interaction (FSI) responses of the splashdown event of a WLO were evaluated. The numerical predictions are first validated with experimental data for maximum impact accelerations and then used to supplement experimental drop tests to establish trends over a wide range of conditions including variations in vertical velocity, entry angle, and object weight. The numerical results show that the fully coupled FSI models can capture the water-impact response accurately for all range of drop tests considered, and the impact acceleration varies practically linearly with increase in drop height. In view of the good comparison between the experimental and numerical simulations, both models can readily be employed for parametric studies and for studying the prototype splashdown under more realistic field conditions in the oceans. [DOI: 10.1115/1.4027454]

Introduction

Ocean entry dynamics of a generic WLO is an intrinsic component of many naval applications. Examples include ship slamming, torpedo water entry, and space module water landing impact analysis. The recent emphasis of the Navy on Intelligent, Surveillance and Reconnaissance, Mine Warfare, Naval Special Warfare, and Anti-Submarine Warfare further highlights the importance of multiphysics numerical codes capable of modeling the ocean environment and contact/impact phenomena of deployed systems accurately. The present study is concerned with numerical analysis of the ocean water landing of a generic rigid object (WLO) and its comparison with the experimental results. The effect of this impact is often prominent in the design phase of re-entry projects, to determine the maximum force for material strength determination to ensure structural and equipment integrity and human safety.

Prototype data (generic shape and dimensions) has been provided by the Indian Space Research Organization to facilitate the development of a physical WLO model. The shape of the prototype is unique in a way that it is conical with a rounded nose (which impacts the water surface first) than compared to the convex shape of the base used for American space missions. This significantly inhibits the comparison with the literature available for Apollo command module or other American space missions.

Studies on impact phenomena based on the theoretical and experimental work by von Karman [1] and Wagner [2] resulted in approximate estimates and bounds for the impact accelerations on rigid bodies entering water free surface. Using an expression for the added mass of the water, acceleration of and pressure on the

rigid body were determined. Miloh [3] obtained analytical expressions for the small-time slamming coefficient and wetting factor of a rigid spherical shape in a vertical water entry. A semi-Wagner approach was then used to compute the wetting factor and the Lagrange equations were employed in order to determine the slamming force from the kinetic energy of the fluid. Good agreement between theoretical model and experimental measurements, both for the early-stage impact force and the free-surface rise at the vicinity of the sphere was observed. Brooks and Anderson [4] investigated the dynamic response of water-landing space module during impact upon water. A 1/5th-scale model was tested in a three-dimensional (3D) basin at the Hinsdale Wave Research Laboratory at Oregon State University (OSU) and the results were compared with those obtained using analytical techniques and computer simulations. The 3D FE model was validated by comparison with previous full-scale test data and theory. Zhao et al. [5] developed a generalized Wagner model, within which only the boundary conditions (BCs) on the fluid free surface are simplified (linearized BCs). Faltinsen [6] studied the relative importance of hydroelasticity for an elastic hull with wedge-shaped cross sections penetrating an initially calm water surface. Wagner's theory was generalized to include elastic vibrations. The importance of hydroelasticity for the local slamming-induced maximum stresses was found to increase with decreasing deadrise angle β and increasing impact velocity V. Fair agreement between theory and experiments was documented. Scolan and Korobkin [7] considered the 3D problem of a blunt-body impact onto the free surface of an ideal incompressible liquid based on Wagner's theory. They also found that the bounds on maximum acceleration due to impact of a rigid object water re-entry can be obtained analytically. Souli et al. [8] evaluated the capabilities of FSI and ALE formulation for various fluid dynamics problems and showed that FE code is an efficient tool for analyzing large deformation processes with its multimaterial ALE capabilities. Korobkin and

Scolan [9] also performed hydroelastic slamming analysis of a 3D cone using Wagner's approach. Tutt and Taylor [10] assessed the performance of recovery vehicles in the event of a water landing. They investigated the application of the Eulerian-Lagrangian penalty coupling algorithm and multimaterial ALE capabilities for the water impact. Melis and Bui [11] studied the ALE capability to predict splashdown loads on a proposed replacement/upgrade of hydrazine tanks on a thrust vector control system housed within the aft skirt of a Space Shuttle solid rocket booster. Preliminary studies on the booster impacting water showed that useful predictions can be obtained using the ALE methodology to a detailed analysis of a 26 deg section of the skirt with a proposed tank attached. The 3D nonlinear theory of water impact was solved by Korobkin [12] using a modified Logvinovich model, which is slightly more complex than the Wagner's method used in this study. Seddon and Moatamedi [13] reviewed water entry studies between 1929 and 2003, and provided a summary of major theoretical, experimental and numerical accomplishments in the field. Wang and Lyle [14] simulated space capsule water landing using an ALE FE solver and a penalty coupling method to predict fluid and structure interaction forces. The capsule was assumed rigid and results were found to correlate well with closed-form solutions. Jackson and Fuchs [15] conducted vertical drop tests on a 5 ft diameter composite fuselage section into water. A detailed FE model was developed to model the impact event using the ALE and SPH approaches in LS-DYNA. Vandamme et al. [16] investigated the fluid and floating object interaction using a novel adaptation of the weakly compressible smoothed particle hydrodynamics method by incorporating a floating object model. Simulations results for water entry and exit of a buoyant and neutral density cylinder showed good agreement with previous experimental, numerical, and empirical studies in penetration depth, free surface motions, and object movement.

It is apparent that though FE codes were used for many fluid-structure interaction problems in the past, modeling the air and water domains accurately in such problems still poses difficulties. A general-purpose nonlinear transient dynamic finite element code for analyzing large deformation rate response of fluids including fluids coupled to structures is used in the present study. Dynamic behavior of the WLO dropped from specific heights (with varying entry speed and weight) to provide data for calibration of prediction results from numerical studies is examined in this article. Experimental and numerical results are correlated with classical solutions using the von Karman and Wagner approaches for maximum impact acceleration.

Finite-Element Modeling of the Experimental WLO Drop Tests

The present paper is the second of a two-part series to investigate the water entry dynamics of a rigid body, both experimentally and numerically. It constitutes the first part of a project in which two independent sets of experiments were conducted to calculate the maximum impact accelerations and touchdown pressures on a WLO upon impact with water surface [17]. Drop Test I involved dropping the object using a rope and pulley arrangement, while Drop Test II employed an electromagnetic release to drop the model [17]. In this article, the numerical study of the dynamic response of a WLO water impact is presented for both drop test cases. Both sets of experiments provide valuable and complementary experimental data (for different weight distribution ratios) for numerical model validation. Both test cases involved dropping the object over a range of 0.5 m intervals where the maximum permissible height of 5 m corresponds to an achievable velocity of 9.81 m/s.

To simulate the dynamic response of the impact experiment for model testing, a 1/6th Froude scale model of WLO [made of fiber reinforced plastic (FRP)] was used [17]. The overall configuration of the WLO prototype is shown in Fig. 1. Note that the conical portion (nose part of the rigid-object) impacts the water surface
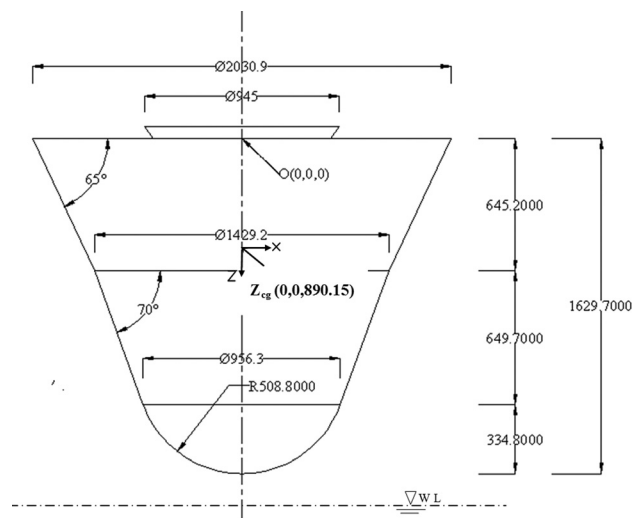

Fig. 1 Overall configuration of WLO prototype (all dimensions are in mm)

first. The origin of reference is located at the deck of the WLO and the position of Z_{cg} is measured from the flat base (Fig. 1). The scaled model of the WLO has a maximum base diameter of 338.5 mm and a height of 271.6 mm. The weight of the WLO is 2.03 kg. A skin thickness of 5 mm was selected, with extra thickness at the nose (of about 10 mm) to withstand the force of impact.

A numerical code for nonlinear dynamic analysis of structures in 3D, LS-DYNA, is used in the current study (Version: mpp971d R7.0.0 and Revision: 79055). The predictive capability of the nonlinear explicit dynamic finite element code is evaluated. This work utilizes the built-in contact-impact algorithm along with the ALE and SPH features to simulate the fully coupled FSI phenomenon. More details on the version, number of degrees of freedom and the platforms used are presented in the *performance studies of ALE and SPH* section.

For the problem considered, the dynamic response involves the penetration of the object treated essentially as a rigid body through the air/water domain. All the ALE simulation models involve three components: (i) WLO, (ii) air domain, and (iii) water domain. Note that all the numerical tests were confined to vertical impact only. For information on the effect of horizontal speed of the entering body, see Ref. [18].

The air and water domains were modeled using solid brick elements in an axisymmetric cylindrical domain. An important feature in simulating contact and impact problems is proper modeling of the two-phase flow including the presence of air. A common practice of past studies in modeling the air domain in coupled FSI contact and impact problems is to use either "vacuum" or "void material" to model the air domain. However, this does not capture the physics accurately and leads to unrealistic high impact accelerations. In this paper, we include air modeling using material properties and a governing equation of state.

The Apollo-like space capsule (used for many previous impact studies) and by Wang and Lyle [14] had a maximum diameter of 198 in. (~5 m) and a height of 130 in. (~3.3 m). The weight is estimated to be 16,200 lbs (~7348 kg). The FE computational setup for such a model demands large water and air domains requiring a very larger number of nodes and elements to achieve convergence. However, in the present study the maximum diameter of the 1/6th Froude-scale model of the WLO is 338.5 mm and a height of 271.6 mm with a weight of 2.03 kg. Hence, a water body of 4 m (diameter) × 2 m (length) and an air domain of 4 m (diameter) × 1.0 m (length) are modeled for the impact studies. Null material model which has very little shear strength is used to model the water and air domains with a mass density of

$1000 \, \text{kg/m}^3$ and $1.29 \, \text{kg/m}^3$, respectively, which needs an equation of state to be defined.

The WLO is made up of FRP and the mass density and Young's modulus values are those of the FRP material used for both experimental test cases and numerical simulations. The WLO is treated as a rigid body with a mass density of $1764.52 \, \text{kg/m}^3$. (As a side note and for completeness of information, in the numerical computation of the coupled fluid-rigid body interaction, the code uses a penalty function method to determine the location of the common contact surface between the fluid and the rigid body that requires the input of artificial values of Young's modulus and Poisson's ratio of the body to compute the penalty function spring stiffness for intermediate iterations. For the simulations performed in this study, a Young's modulus of $4.895 \times 10^9 \, \text{N/m}^2$ and a Poisson ratio of 0.2 appear to be optimal.)

Eight-node brick elements and 4-node Belytschko-Lin-Tsay shell elements [19,20] are used for discretization of the air/water and WLO domains, respectively. A constrained Lagrange interface/contact is used to model the impact event between the object (treated as a rigid body) and the air-water target. In this, the moving surface of 3D rigid body (a Lagrangian mesh) is treated as the slave surface, and the target air-water mesh is treated as the master surface.

Importantly, Navier—Stokes equations and ALE formulations are solved over the entire computational domain. In the ALE description, an arbitrary referential coordinate is introduced in addition to the Lagrangian and ALE coordinates [21]. The material time derivative of a variable with respect to the reference coordinate can be described as

$$\frac{dg(\vec{X},t)}{dt} = \frac{\partial g(\vec{x},t)}{\partial t} + \rho(\vec{v} - \vec{w}).\overrightarrow{\text{grad}}g(\vec{x},t) \quad (1)$$

where $\vec{X}$ is the Lagrangian coordinate, $\vec{x}$ is the ALE coordinate, $\vec{v}$ is the particle velocity, and $\vec{w}$ is the grid velocity of the numerical simulation. The ALE differential form of the conservation equations for mass, momentum, and energy are readily obtained from the corresponding Eulerian forms

$$\text{Mass}: \frac{\partial \rho}{\partial t} + \rho \text{div}(\vec{v}) + (\vec{v} - \vec{w})\text{grad}(\rho) = 0 \quad (2)$$

$$\text{Momentum}: \rho \frac{\partial \vec{v}}{\partial t} + \rho(\vec{v} - \vec{w}).\overrightarrow{\text{grad}}(\vec{v}) = \overrightarrow{\text{div}}(\overline{\overline{\sigma}}) + \vec{f} \quad (3)$$

$$\text{Energy}: \rho \frac{\partial e}{\partial t} + \rho(\vec{v} - \vec{w}).\overrightarrow{\text{grad}}(e) = \overline{\overline{\sigma}} : \overline{\overline{\text{grad}}}(\vec{v}) + \vec{f}.\vec{v} \quad (4)$$

where ρ is the mass density, $\vec{f}$ is body force vector, and e is the total energy. $\overline{\overline{\sigma}}$ denotes the total Cauchy stress given by

$$\overline{\overline{\sigma}} = -p\overline{\overline{I}} + \mu(\overline{\overline{\text{grad}(\vec{v})}} + \overline{\overline{\text{grad}(\vec{v})}}^T) \quad (5)$$

where p is the pressure, $\overline{\overline{I}}$ is the identity tensor, μ is the dynamic viscosity, and $(\vec{v} - \vec{w})$ is the convective velocity across the grid.

The elements of the air and water domains were given the null hydrodynamic material type that allowed a new equation of state to be specified. An equation of state with a linear polynomial form is used to define the initial thermodynamic state of the material and pressure [20] is given by

$$p = C_0 + C_1\zeta + C_2\zeta^2 + C_3\zeta^3 + (C_4 + C_5\zeta + C_6\zeta^2)E \quad (6)$$

where C_{0-6} are user-defined constants, E is initial energy per initial volume, and the volumetric parameter ζ is defined as

$$\zeta = \frac{1}{V} - 1 \quad (7)$$

where V is relative volume given as

$$V = \frac{\rho_0}{\rho} \quad (8)$$

With ρ_0 as the reference mass density (which might be different than the current mass density if the material experiences compression or expansion throughout the simulation). The constant C_1 in Eq. (6), when used by itself, is the elastic bulk modulus ($C_1 = \rho * c_s^2$), where ρ is the mass density of the material and c_s is the sound speed in air/water ($c_s = 1480 \, \text{m/s}$ for water and $c_s = 343 \, \text{m/s}$ for air). Providing this constant only and setting all other constants to zero is sufficient to define the equation of state if the pressure is not significantly influenced by temperature changes.

As another side note, sound speed in water plays a significant role in determining the integration time step and also the total computational time. The time step can be artificially lowered for fluids without affecting the accuracy of the fluid motion computation but can significantly reduce the computational effort by allowing a significantly large time step [22]. A sound speed $100 \, \text{m/s}$ is employed in all subsequent computations in this study. This provides values of C_1 for air and water domains are $1.0 \times 10^{+05} \, \text{N/m}^2$ and $1.0 \times 10^{+07} \, \text{N/m}^2$, respectively.

The boundary conditions employed in the numerical model are partially the material surfaces (out-of-plane, in-plane and bending restraint). The material surfaces defined in ALE formulation are: (a) no particles can cross them and (b) stresses must be continuous across the surfaces.

Finite-Element Simulations. A number of model development techniques were examined to identify the most efficient and accurate models, some of which are discussed here.

Modeling Air. An air pressurization study was conducted to confirm that the magnitude of the pressure in the air is necessary to not only energize the air around the rigid body but also to get a good velocity contour around the falling object, making it is a significant parameter in modeling these kind of contact and impact problems.

Rigid-Body Starting Location. A review of the starting location of the rigid body was performed. It was clear that the rigid body (with prescribed initial velocity) would need to fall from a height large enough to allow the surrounding air flow to be captured accurately but not so large as to require a very large computational domain (and hence simulation time) that does not improve the predictive accuracy. It was found that starting location of $0.3 \, \text{m}$ above the water surface with a corresponding initial velocity (obtained from analysis) was adequate for all the rigid body impact tests to accurately capture the physics of the impact. Note that the mesh of the WLO is immersed in the Eulerian meshes of water and air, but the fluid nodes and the structure do not need to be coincident.

Mesh Size Variation. The mesh size of the ALE air and water domains close to the impact zone were varied from a coarse $100 \, \text{mm}$ grid to a fine mesh of $20 \, \text{mm}$ grid to study the convergence of the peak impact acceleration values.

Simulations were performed over a wide range of conditions. The characteristics of entry speed, entry angle, and vehicle weight were varied. The time step was approximately 3.0×10^{-05} s. There were a total of 732,550 nodes and 714,180 in the 3D ALE model. For each simulation, a total of 33,246 data states were created from the simulation. Displacement, velocity, and acceleration of the model were recorded (related to the center of mass of WLO). An important result from these simulations is the maximum impact acceleration sand maximum impact pressures experienced by the object upon impact for each drop height. Figures 2(a) and 2(b) show the plan and top view of the computational
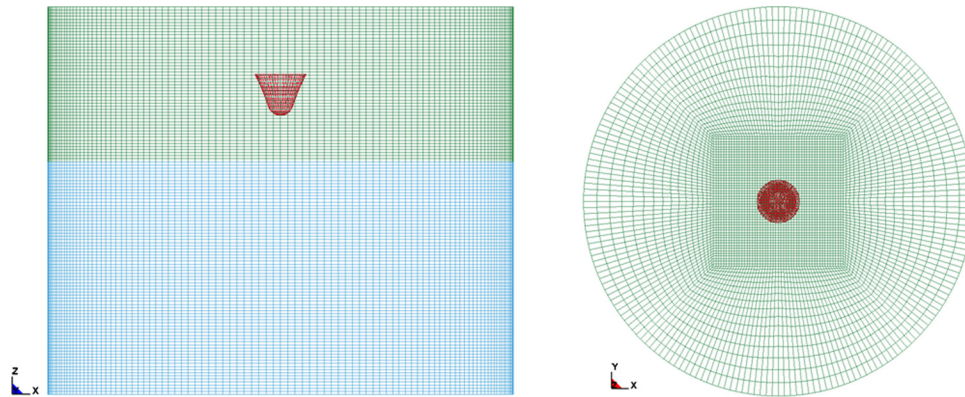
Fig. 2 (*a*) and (*b*) Elevation and top view of the FE-ALE computational mesh (top part is the air domain; bottom part is the water domain; and the rigid body in the air domain is the WLO model)
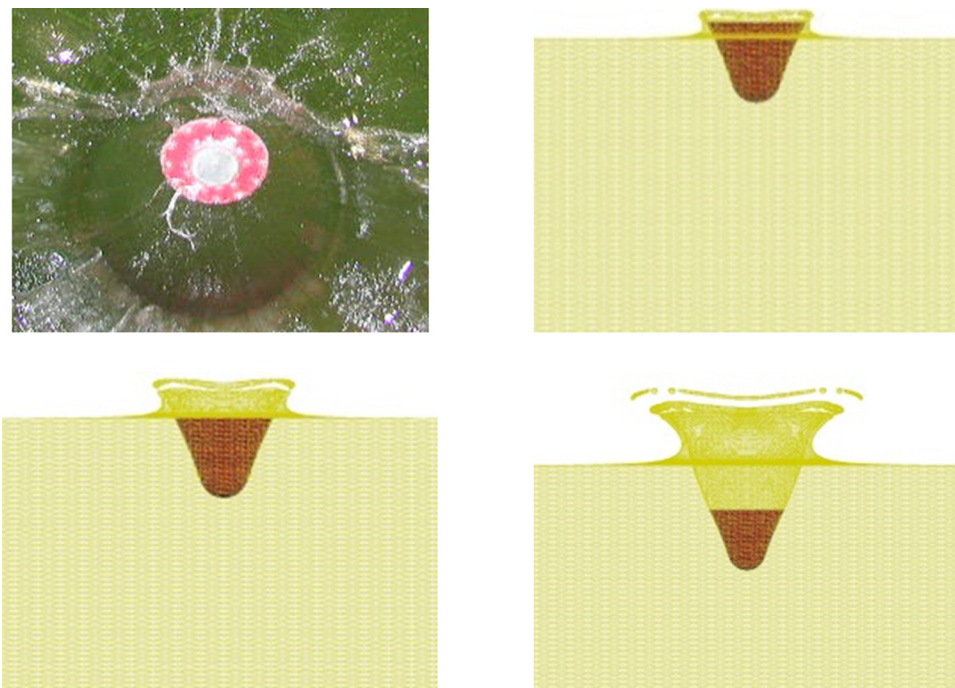

Fig. 3 Animation images at various time steps for vertical impact

mesh. In all numerical simulations the accelerations are obtained in reference to the local *Z* direction, unless indicated otherwise.

Effects of Vertical Velocity Variation. The vertical velocities of the WLO considered in this study varied from 9.8 m/s to 4.4 m/s (with 9.8 m/s corresponding to Drop Test-I). Figure 3 shows the animation images of the impact at various time steps in comparison to the image from the experiment shown exactly during impact.

Figures 4 and 5 show acceleration and pressure time histories for a 5 m drop test. It can be observed that the modeling of the two-phase flow with the proper simulation of the dynamics of air provides accurate impact acceleration results that are remarkably close to the WLO experimental impact data, providing a high degree of confidence in the applicability of ALE methodology to this class of intricate contact and impact problems. For a 5 m drop height, Fig. 4 shows that the peak acceleration upon impact corresponds to 55.10 m/s^2 (5.5 g) and Fig. 5 shows that the peak impact pressure corresponds to 28 KPa. Note that the pressure acting on a

rigid body is computed using an inbuilt FSI sensor (placed strategically at the nose of the WLO impacting water surface first).

The acceleration and pressure time histories (Figs. 4 and 5) also depicts that during free fall, the response remains flat ($0 < t < 0.245$ s), due to the positioning of the rigid body with respect to the water surface and during touchdown on the water surface the acceleration and pressure peaks are recorded ($0.245 < t < 0.254$ s). It is evident from the post impact scenario that the rigid body bounces (with its nose up) after impact ($0.254 < t < 0.55$ s) and subsequently comes to a static equilibrium with a practically constant submerged pressure ($0.55 < t < 1$ s).

Note that, in contrast to the results presented in Refs. [4,14,15], the numerical predictions presented in Figs. 4 and 5, which match well with experiment measurements, do not contain any high frequency oscillatory "noise" and does not require filtering. We attribute this improvement in the predictive capability to the accurate modeling of the behavior of air flow around the rigid body.

An attempt was made to measure the maximum depth of immersion of WLO after impact using the experiments but they were discarded as they were deemed unreliable. A tracer particle
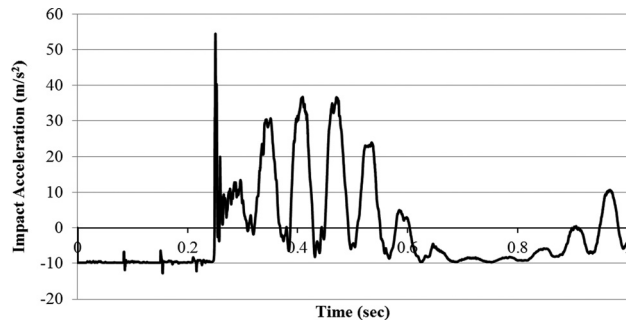
Fig. 4 Numerical simulation response of a 5 m drop test: (a) acceleration time history
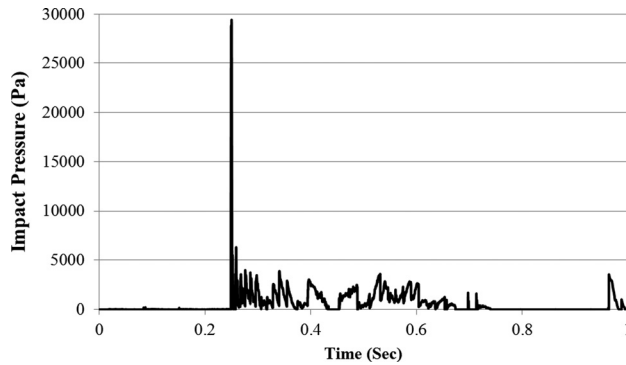

Fig. 5 Numerical simulation response of a 5 m drop test: (b) pressure time history
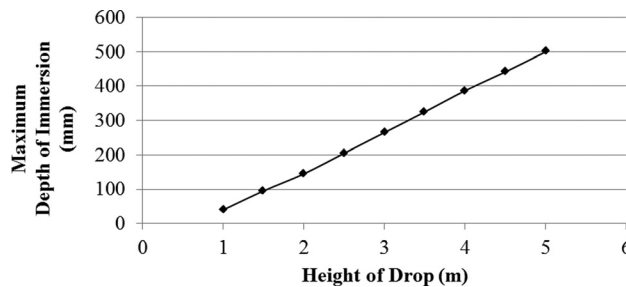

Fig. 6 Height of drop versus depth of Immersion for case-I

approach using a tracer node is used to measure the depth of immersion in the numerical simulations. Figure 6 shows a linear relationship between the depth of immersion and the drop height.

Table 1 shows a comparison of experimental data (Drop Test-I: mechanical release) with the ALE predictions. Due to the highly

Table 2 Summary of the pitch tests (V = 9.8 m/s) (weight of WLO = 2.03 kg)

Entry angle (deg)	Maximum impact acceleration (Numerical) (m/s²)	Maximum impact pressure (Numerical) (KPa)
0	55.10	28.12
15	45.75	17.92
30	32.01	11.45
45	15.55	9.50

stochastic nature of the peak pressure estimates on the rigid body [23], each drop test was repeated thrice and the maximum impact pressure reported in Table 1 is the mean value of three drop test cases.

Effects of Entry Angle Variation. The entry angles of the WLO upon impact were varied from 15 to 40 deg (Table 2) to examine its influence on peak acceleration. Simulation results show that the impact acceleration can be reduced by having the WLO enter the water at an angle.

Note that the experimental studies did not involve pitch tests [17]. When the local dead rise angle (β) between the water surface and the dropping object is not very small at the impact position, the body can be assumed rigid in the hydrodynamic calculations [23]. The relatively high stiffness of the scaled down model is due to the rigid body definition. When β is small, the hydroelastic effects become important [6,23] and the maximum impact accelerations are greatly affected by the hydroelastic interactions at impact [14]. Previous studies on water impact analysis involved objects with small β compared to the present scenario which deals with a unique shape of the WLO with a large β during impact with water surface. This is one of the reasons for the excellent comparisons between the experimental and numerical test data.

Effects of Weight Variation. The effects of variations in the weight of the WLO on maximum impact acceleration and pressure was examined by varying the object weight from 2.5 kg to 5 kg (3.5 kg corresponds to Drop Test-II involving an electromagnetic drop mechanism). Trends obtained from acceleration and pressure time histories for a 3.5 kg model were similar to those obtained for Drop Test-I [17]. The acceleration time history for a weight of 3.5 kg of WLO yields a peak impact acceleration value of 38.20 m/s² (3.8 g) and a touchdown pressure of 43.5 KPa. Table 3 shows a comparison of experimental results from the electromagnetic release mechanism with the ALE formulation. The peak accelerations obtained from the FE simulations and the experimental data for Drop Test–II are 38.20 m/s² and 36.50 m/s², respectively, showing good predictive capability of the numerical model.

Analytical Description of the General Contact–Impact Problem. For a rigid object with a spherical bottom, closed-form solutions based on the von Karman and Wagner approaches are

Table 1 Simulation results for maximum impact acceleration [Drop Test-I: weight of WLO = 2.03 kg (vertical entry/entry angle = 0 deg)]

Vertical velocity at impact (m/s)	Maximum impact acceleration (Numerical) (m/s²)	Maximum impact acceleration (Experimental) (m/s²)	Maximum impact pressure (Numerical) (KPa)	Maximum impact pressure (Experimental) (KPa)
9.80	55.10	52.17	28.12	26.10
9.27	52.48	48.32	26.61	23.25
8.61	49.32	45.18	23.42	22.15
8.26	39.80	38.76	22.35	19.25
7.55	38.18	37.78	19.75	18.65
6.87	34.18	33.53	18.11	16.35
6.20	32.10	30.27	16.98	15.20
5.31	24.75	22.86	15.45	13.10
4.39	12.58	11.65	14.20	12.80

Table 3 Simulation results for maximum impact acceleration [Drop Test-II: weight of WLO = 3.5 kg (vertical entry/entry angle = 0 deg)]

Vertical velocity at impact (m/s)	Maximum impact acceleration (Numerical) (m/s^2)	Maximum impact acceleration (Experimental) (m/s^2)	Maximum impact pressure (Numerical) (KPa)	Maximum impact pressure (Experimental) (KPa)
9.72	38.20	36.50	43.50	41.15
9.30	32.85	31.72	42.35	38.20
8.81	28.20	27.32	35.70	32.75
8.19	24.80	22.82	31.65	29.35
7.54	22.35	19.55	26.22	25.15
6.97	18.50	15.32	23.17	21.25
6.22	15.10	12.12	20.85	19.10
5.35	11.75	10.72	19.85	18.45
4.42	10.90	9.92	17.33	15.75

Table 4 Analytical solution results from von Karman and Wagner approaches

WLO experimental cases Cone radius: 0.0848 m Max. Radius: 0.3385 m	Maximum acceleration g: acceleration due to gravity (m/s^2)		Analytical solutions for maximum accelerations		Equivalent radius of WLO conical portion (m)	
	Experimental (Drop tests)	Numerical (FE tests)	von Karman (Eq. (5))a_{max}	Wagner (Eq. (10)) a^*_{max}	von Karman r_{max}	Wagner r^*_{max}
Drop Test-I: mechanical mechanism	5.2 g	5.5 g	14.7 g	19.8 g	0.0300 m	0.1075 m
Drop Test-II: electromagnetic release mechanism	3.6 g	3.8 g	10.4 g	25.2 g	0.0293 m	0.1310 m

available to correlate with results from the explicit finite element analyses [14]. The von Karman approach is based on conservation of momentum and uses an added mass [1]. The penetration depth is determined without considering water splash-up. The Wagner approach uses a more rigorous fluid dynamic formulation and includes the effect of water splash-up on the impact force [2]. From the analytical solutions for a spherical bottom body impacting with water using the von Karman method [24], the magnitude of the virtual mass for a spherical bottom body is given by

$$m_v = \frac{4}{3}\rho h^{\frac{3}{2}}(2R - h)^{\frac{3}{2}} \tag{9}$$

where m_v is the virtual mass, ρ is the mass density of water, h is the water depth, and R is the radius of the spherical bottom.

Assuming $(h/R) << 1$, the maximum acceleration can be found as

$$a_{max-vK} = -\frac{256}{243}\left(\frac{4\rho g R^3}{3W}\right)^{\frac{2}{3}}\left(\frac{V_0^2}{R}\right) \tag{10}$$

where vK stands for von Karman in above equation.

A semi-Wagner approach to determine the nondimensional slamming coefficient [3] is based on these analytical derivations the maximum acceleration can be estimated as

$$a_{max-W} = \frac{g}{2W}C_s\left(\frac{h_{max}}{R}\right)\rho\pi R^2 V_0^2 \tag{11}$$

where W stands for Wagner above equation.

The equivalent radius is a representative or nominal radius of WLO that yields the accelerations comparable to the maximum impact accelerations obtained experimentally with the conical shaped WLO [17]. From the analytical solutions for a spherical bottom body impacting with water surface, for the von Karman method, Eq. (10) is used to calculate the equivalent radius by computing r_{max-vK} corresponding the maximum impact acceleration a_{max-vK} and is given by

$$r_{max}-vK = R = -\frac{a_{max}-vK}{V_0^2}\left(\frac{243}{256}\right)\left(\frac{3W}{4\rho g}\right)^{\frac{2}{3}} \tag{12}$$

and correspondingly for the Wagner method, Eq. (11) can be used to calculate the equivalent radius by computing the value of r_{max-W} corresponding the maximum impact acceleration a_{max-W} and is given by

$$r_{max-W} = R = \frac{2Wa_{max-W}}{\rho g\pi V_0^2 C_s h_{max}} \tag{13}$$

Values of the "equivalent radius" of the WLO conical portion is also shown in Table 4. A detailed description of the equivalent radius approximate semi-analytical procedure is provided in [17]. Table 4 also shows a comparison of the FE simulation results (Drop Test-I and Drop Test-II) with analytical solutions using von Karman and Wagner approaches and experimental test data.

It is important to note that the maximum radius of the base (for a 1/6th Froude-scale model of WLO) is 338.5 mm and the radius of the conical portion impacting the water surface is 84.8 mm. For a conical bottomed rigid object, the FE results show that there is large difference between the numerical peak impact accelerations and those obtained by von Karman and Wagner analytical estimates. This large difference can be attributed to the conical shape of WLO bottom impacting the water surface compared to the large spherical bottom used in deriving the closed-form solutions. In addition to the unique shape of the WLO the basic assumptions of the formulations for both the von Karman and Wagner approaches also play a pivotal role in contributing to the large difference. The von Karman approach is based on the momentum theorem (using an added virtual mass) and the penetration depth is determined without considering the splash-up of the water level, thus neglecting the highly nonlinear coupled fluid-structure interaction effect. The Wagner approach, on the other hand, attempts to relax the von Karman no-splashing assumption by using a rigorous dynamic formulation and incorporates the effect of the upward splashing of the water and its effects on the object. With the upward splashing correction, the Wagner approach tends to

over predict the maximum impact retardation as it neglects the water compressibility (i.e., a more yielding fluid) near the impact zone. The lack of agreement in the maximum impact accelerations obtained in the present numerical study with the closed-form von Karman and Wagner approximate solutions is due to the large initial angle at impact and the relatively rapid changes in contact radius of the inverted cone shape of the WLO as it penetrates the water surface. These deviations from the idealized assumption may be taken into account using the concept of an equivalent radius [17].

SPH Simulations

SPH is an N-body integration scheme initially developed by Gingold and Monaghan [25] and Lucy [26] to avoid the limitations of mesh tangling encountered in extreme deformation problems with the FE method. The main difference between classical methods and SPH is the absence of grid. Hence, the particles constitute the computational framework on which the governing equations are resolved. The main advantage arises directly from its Lagrangian nature, since such an approach can tackle difficulties related with lack of symmetry, large voids that may develop in the field, and a free water surface much more efficiently than Eulerian methods. The conservation laws of continuum fluid dynamics, in the form of partial differential equations, are transformed into particle form by integral equations through the use of an interpolation function that gives kernel estimation of the field variables at a point [20]. Null material model with an equation of state is used to model the water domain. The speed of sound at the reference density was set to 100 m/s as the acoustic speed is not important for the present problem. It is worthy to note that this sound speed is much lower than that of water, but much faster than the water wave propagation in the model.

SPH Formulation. The particle approximation function is given by

$$\prod{}^{h} f(x) = \int f(y) W(x - y, h) dy \qquad (14)$$

where W is the kernel function. The Kernel function W is defined using the function θ by the relation

$$W(x, h) = \frac{1}{h(x)^{d}} \theta(x) \qquad (15)$$

where d is the number of space dimensions and h is the so-called smoothing length which varied in time and space. $W(x, h)$ is a centrally peaked function. The most common smoothing kernel used by the SPH is the cubic B-spline which is defined by choosing θ as

$$\theta(u) = Cx \begin{cases} 1 - \dfrac{3}{2} u^{2} + \dfrac{3}{4} u^{3} & \text{for} \quad |u| \le 1 \\ \dfrac{1}{4}(2 - u)^{3} & \text{for} \quad 1 \le |u| \le 2 \\ 0 & \text{for} \quad 2 < |u| \end{cases} \qquad (16)$$

where C is a constant of normalization that depends on the spatial dimensions.

The particle approximation of a function is now defined by

$$\prod{}^{h} f(x_i) = \sum_{j=1}^{N} w_j f(x_i) W(x_i - x_j, h) \qquad (17)$$

where $w_j = (m_j / \rho_j)$ is the "weight" of the particle. The weight of a particle varies proportionally to the divergence of the flow.

Discrete Form of Conservation Equation. The conservation equations are written in their discrete form and the momentum conservation equation is

$$\frac{dv^{\alpha}}{dt}(x_i(t)) = \frac{1}{\rho_i} \frac{\partial(\sigma^{\alpha\beta})}{\partial x_i}(x_i(t)) \qquad (18)$$

where α, β are the space indices.

Energy conservation equation is given by

$$\frac{dE}{dt} = -\frac{P}{\rho} \nabla v \qquad (19)$$

Artificial Viscosity. The artificial viscosity is introduced when a shock is present. Shocks introduce discontinuities in functions. The role of artificial viscosity is to smooth the shock over several particles. To take into account the artificial viscosity, an artificial viscous pressure term Π_{ij} is added such that

$$p_i \rightarrow p_{i+} \Pi_{ij} \qquad (20)$$

where $\Pi_{ij} = (1/\bar{\rho}_{ij})(-\alpha\mu_{ij}\bar{c}_{ij} + \beta\mu_{ij}^2)$. The notation $X_{ij} = (1/2)(X_i + X_j)^-$ is used for median between X_i and X_j, c is the adiabatic sound speed, and

$$\mu_{ij} = \begin{cases} \bar{h}_{ij} \dfrac{v_{ij} r_{ij}}{r_{ij}^2 + \eta^2} & \text{for} \quad \nu_{ij} r_{ij} < 0 \\ 0 & \text{otherwise} \end{cases} \qquad (21)$$

Here, $v_{ij} = (v_i - v_j)$, and $\eta^2 = 0.01 \bar{h}_{ij}^2$ which prevents the denominator from vanishing.

Time Integration. A simple and classical first-order scheme for integration is used. The time step is determined by the expression

$$\delta t = C_{\text{CFL}} \text{Min} \left(\frac{h_i}{c_i + v_i} \right) \qquad (22)$$

where the factor C_{CFL} is a numerical constant.

Description of the SPH Model. Water was simulated by using SPH elements. There is no need for the modeling of the air domain in SPH. A water body of 4 m (diameter) × 2 m (height) was modeled as a cylindrical mesh, was chosen for the impact studies (number of SPH particles/nodes = 1,23,570). The edges of the water were defined as fixed-SPH nodes allowing the water block to be relatively small in size. Figure 7 shows the plan of the SPH particle setup. The same material properties that were used in the ALE simulations were retained for the rigid object and the water domain for the SPH simulations.

Effects of Vertical Velocity Variation. The vertical velocities ranged from 9.8 m/s to 4.4 m/s, of which 9.8 m/s corresponds to Drop Test-I. SPH animation images of particle impingement (by the rigid body) are shown in Fig. 8. Acceleration time history for a 5 m drop test (Fig. 9) shows that the maximum impact acceleration is approximately 49 m/s^2.

Note that the acceleration time history was filtered at 1000 Hz using Butterworth filter (same frequency that was used to sample the experimental results) to remove the high frequency content that is part of modeling water using a compressible fluid solver. Figure 10 shows a good comparison between the experimental and the ALE and SPH results for maximum impact acceleration. The graph indicates that the trend of impact accelerations increases with an increase in the entry speed. Figure 10 also shows the plot of accelerations obtained analytically versus drop height
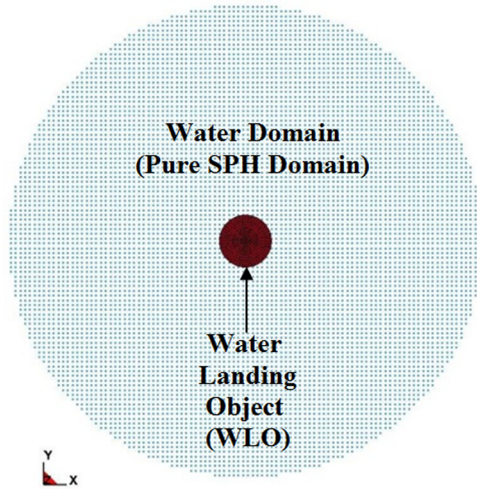
Fig. 7 Plan of the SPH water domain and the WLO (number of SPH nodes: 712,000)

Fig. 9 SPH acceleration time history for a 5 m drop height

for the WLO model (using the original radius of the WLO). It is important to note the values of maximum impact accelerations are almost identical for both von Karman and Wagner solutions.

Effects of Entry Angle Variation (Pitch Tests). To determine the effect of varying the entry angle of the WLO upon impact; the entry angle was varied from 15 to 30 deg. Comparative results with ALE from these tests are shown in Fig. 11. As expected, the impact acceleration can be reduced by having the WLO enter the water surface at an angle. It is also important to note that the SPH results match reasonably well with the ALE results for the inclined impact tests. Though experimental investigation was not carried out for pitch tests to calibrate the numerical predictions, it is nevertheless interesting to observe the closeness of prediction results obtained by the two numerical models. This also demonstrates the usefulness of numerical simulations once the models have been calibrated by other experimental data.

Effects of Weight Variation. Effect of varying the rigid body weight on impact accelerations was studied by varying WLO
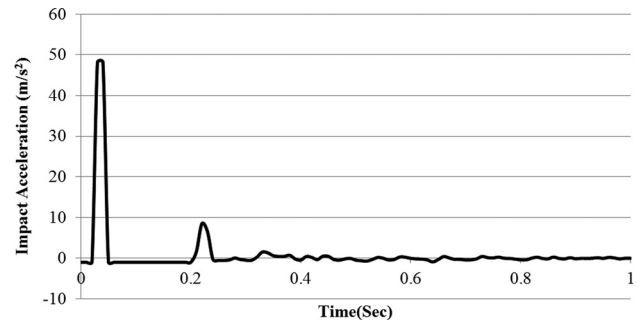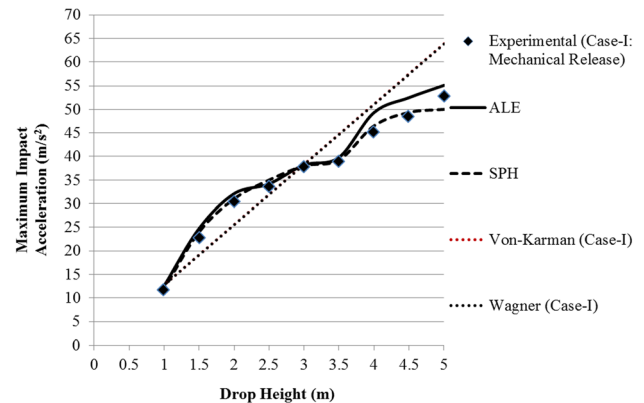

Fig. 10 Comparison of results for maximum acceleration with ALE and SPH [weight of WLO = 2.03 kg (case-I: mechanical release)] (vertical entry/entry angle = 0 deg)

weight from 2.5 kg to 5 kg. A test for 3.5 kg corresponds to Drop Test-II involving an electromagnetic drop mechanism. The general trend shows a small advantage gained in reduced *g*-force for a large increase in weight. Figure 12 shows the comparison of experimental results from the electromagnetic release mechanism with the ALE and SPH formulation. Observe that the peak acceleration decreases linearly with the successive decrease in the
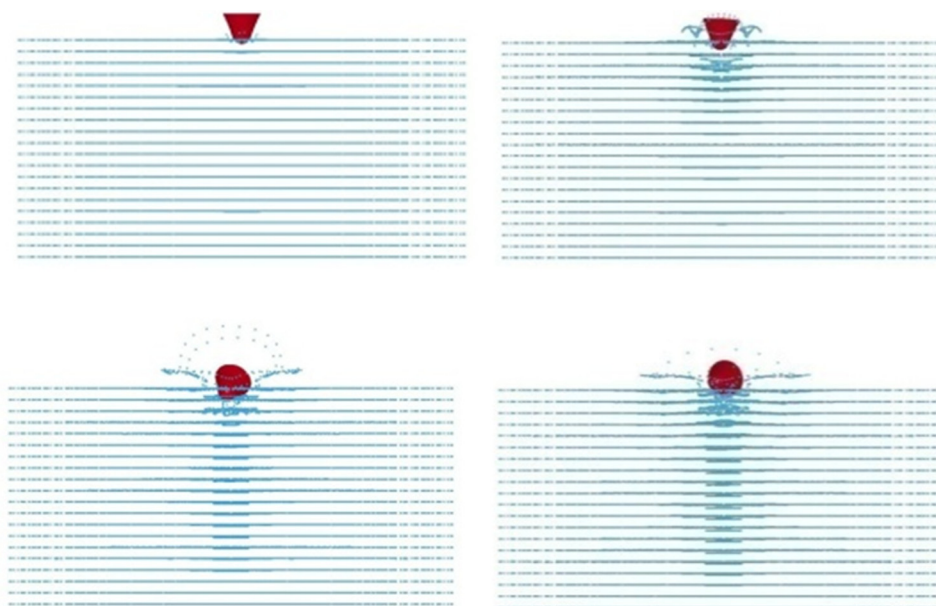

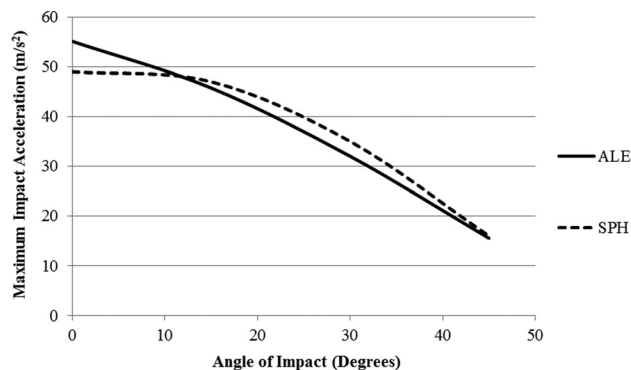**Fig. 8 SPH animation images of the particle impingement at various time steps**

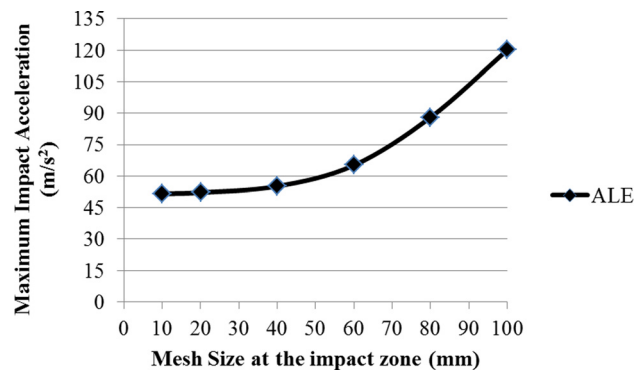**Fig. 11 Comparison of peak impact acceleration for pitch tests using ALE and SPH methods**

Fig. 13 Mesh size variation versus maximum impact acceleration
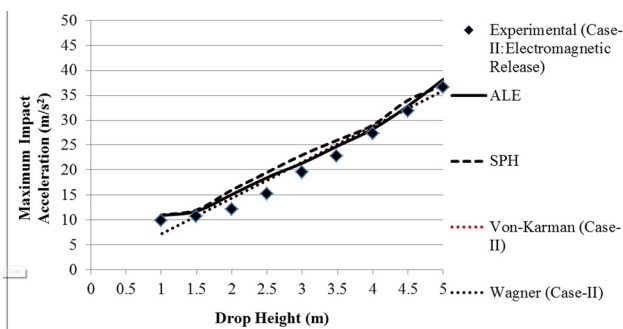

Fig. 12 Comparison of results for maximum acceleration with ALE and SPH [weight of WLO = 3.5 kg (case-II: electromagnetic release)] (vertical entry/entry angle = 0 deg)
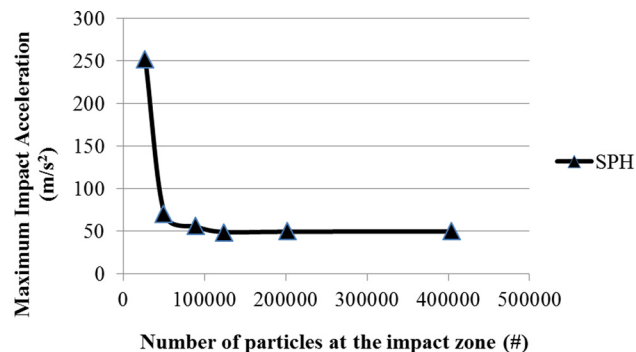

Fig. 14 Number of particles (SPH nodes) versus maximum impact acceleration

height of drop and the peak acceleration is reduced due to the increase in the weight of WLO. Importantly, there is good comparison of the experimental results with both the numerical simulations.

The plot of accelerations obtained analytically versus drop height for the WLO model (using the original radius of the WLO) is also shown in Fig. 12. The plot also depicts that the values of maximum impact accelerations (obtained analytically) are almost similar for both von Karman and Wagner solutions.

Mesh Refinement Studies

To investigate convergence of the numerical solution, a mesh refinement study of the numerical models with a rigid body at a zero-degree pitch angle using different mesh sizes for the impact interaction region, are analyzed (Fig. 13). Mesh sizes coarser than 100 mm near the impact zone not only fail to provide sufficient coupling between the rigid body and the air/water domains but also fails to model the water splash-up very accurately. Figure 13 shows that with a very fine mesh sizes the maximum acceleration values converge, hence, providing confidence in the methodology adopted to simulate the complex event. The values of maximum impact acceleration with variation in the number of SPH particles are shown in Fig. 14. Both figures show that with a finer mesh size the solution for maximum impact acceleration seems to converge but the mesh should be not be too fine to increase the computational time unnecessarily.

Performance Studies of ALE and SPH

Solving practical engineering analysis problems often requires use of large-scale numerical models (which can have several thousands or millions of nodes and elements) and access to the high-performance computing (HPC) platforms to achieve reasonable accuracy. Advanced numerical codes like ALE and SPH need such HPC platforms clubbed with a definitive model size to solve real time 3D FSI problems. Model size plays a pivotal role in not only capturing the physics of the problem but also determines the computational effort needed to reach the full termination time.

In the present case, the code used is a MPP version, i.e., it works on multiple processors. This capability enables us to take full advantage of HPC platforms to model larger domains using fine discretization. A Dell Precision WorkStation 690 with eight nodes (two processor socket quad core), Intel Xeon 3 GHz, 64 GB RAM, and loaded with 64 bit Redhat Linux Enterprise 5 is dedicated as a testbed. This is an example of a shared memory type of computing systems. The platform used is Linux RHEL 5.4 with OS Level of MPICH 1.2.6 Xeon64. Compiler is Intel Fortran 10.1 with a Double Precision (I8R8).

In addition to the model size, the run times also plays a significant role in determining the choice of the numerical code. This inherently provides the end users and scientists to proceed with a balanced approach in making a choice in terms of the available hardware, optimum model size and the accuracy in obtaining satisfactory test results.

The performance of ALE and SPH model tests were studied for the typical case of a vertical impact of the WLO. The ALE test case had 732,552 nodes and 714,180 elements whereas the SPH case had 1,23,570 particles/nodes. The model was run on the OSU HPC platform on various nodes and the estimated clock time was recorded for each run. Table 5 shows the execution time taken to compile the jobs on a single cluster by varying the number of CPUs. It also reports the speedup scale factors [which is the ratio of clock time using a single processor divided by the clock time using multiple processors ($=N_1/N_p$)]. The ratio of execution time for both ALE and SPH are also shown in the performance Table 5.

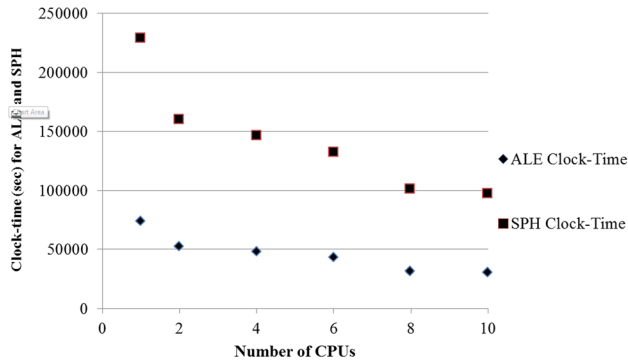| ALE test model: number of time steps = 33,246					
SPH test model: number of time steps = 75,098					
Number of processors (ncpu)	ALE execution time (s)	ALE-speedup (N_1/N_p)	SPH execution time (s)	SPH-speedup (N_1/N_p)	SPH/ALE clock-time ratios
1	73,440	1	229,132	1	3.12
2	51,718	1.42	160,325	1.45	3.10
4	48,315	1.52	146,394	1.65	3.03
6	43,200	1.70	133,056	1.76	3.08
8	31,930	2.30	101,218	2.20	3.17
10	30,347	2.42	97,413	2.25	3.21

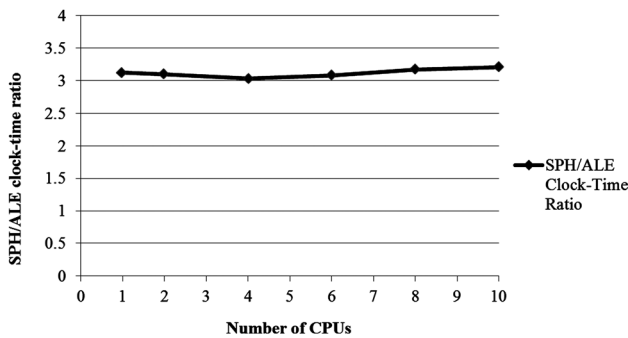Fig. 15 Number of CPUs versus estimated clock time for ALE and SPH test models

Fig. 16 Clock-time ratios of SPH/ALE versus number of CPUs

Fig. 17 Speed scaling of the performance of ALE and SPH (N1/Np)

Discussion and Comparison

The study of hydrodynamic impact between a body in motion and a water free-surface finds variety of applications in the aerospace and ocean engineering fields. The analytical approaches put forth by von Karman, Wagner, and others provide us with the beginnings for a complete solution of the impact phenomena through use of numerical techniques such as finite elements. The effects of varying the vertical velocity, entry angle and the WLO weight were identified and the numerical results obtained from these tests help us understand and establish conditions that must be avoided during the water impact. For instance, if a crew member onboard the WLO cannot withstand impact accelerations over 5 g, these results will give a glimpse of the initial conditions which will keep the peak impact accelerations under the specified limits.

The application of multimaterial Eulerian formulation and a penalty based Lagrangian-Eulerian coupling algorithm combined with a proper working model for both air and water is shown to capture the water landing well. The current work, simulating the complex impact event, using ALE and SPH techniques, demonstrates some of the problems encountered when modeling air and water. The robust contact-impact algorithm of the current FE code simulated the behavior of water for a very short duration of time and the initial period was sufficiently long to establish the trends occurring under a wide range of conditions.

Fluid properties of air and water are defined by the bulk modulus that gives relation between the change of volume and pressure. Reducing the speed of sound in water in the input to the order of about 10 times the celerity of wave, causes a significant reduction in the bulk modulus, thereby resulting in faster execution time as the time step becomes bigger. Because the focus of the wave impact behavior is gravity dominated and not sound propagation sensitive. This technique provides a faster solution without sacrificing accuracy.

Figure 15 graphically illustrate the performance using even number of processors (for two difference numerical methods). Figure 16 graphically demonstrates the ratios of the execution times for both ALE and SPH using number of CPUs. All these figures indicate that as the number of CPUs increases there is a significant reduction in the estimated clock time. The performance studies also reveal that the number of nodes used in the ALE tests is approximately seven times the number of nodes used in the SPH tests, but the ALE formulation is slightly faster than the SPH method. This is due to a very fine ALE mesh size for both the air and water domain. As evident from these figures, the user is now equipped with interesting design choices with the number of processors to achieve an optimal clock time for a given model.

Ideally it is desirable to have linear speedup with respect to the number of processors used to run the model. However, Fig. 17 shows the (speedup) scaling performance of ALE and SPH with increasing number of nodes. Note that scaling performance is far below linear and that they both show a similar trend. Hence, there is little gain in using more than 10 processors for either of the numerical models.
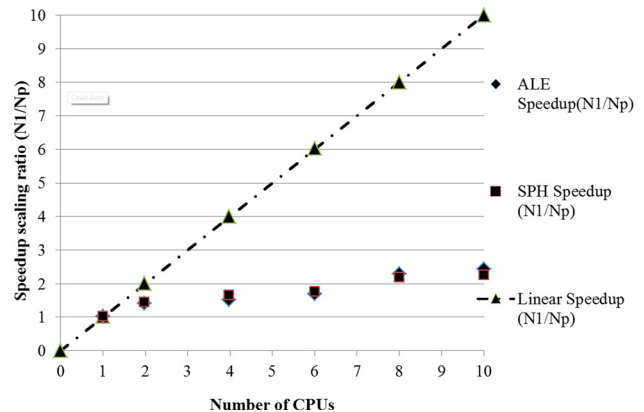
The acceleration values obtained from the simulation results compared well with experimental values. Mesh refinement studies for both the numerical methods showed that maximum impact accelerations converge for a very fine mesh size and are adequate for a good comparative analysis. Importantly, there is a good comparison between the experimental and the ALE and SPH results for maximum impact accelerations for all the three cases of varying the vertical velocity, entry angle, and the weight of the object.

The application of multi material ALE technique and a penalty based coupling algorithm (used for large deformation of water at the free surface upon impact) currently can be properly analyzed only at the cost of high computational time. Use of the SPH method is notably less complicated in generating the model due to the absence of mesh and the ease with which it can successfully model the large deformation problems involving the water domain. The main advantage of using SPH is that it can capture the post impact dynamics (buoyancy effect) more graphically. However, the computational effort required of the SPH method is significantly higher than that of ALE (for multi-phase SPH domains) [16,22,27].

An attempt was made to measure the pressure distribution and the structural deformation coming onto the WLO by treating it as a flexible body, to compare both ALE and SPH codes, but it was discarded due to the high computational time and expense. However, the maximum impact pressure that the WLO is subjected to upon touchdown with the water surface is calculated using an FSI sensor (at the bottom of the WLO) using both the numerical methods.

The WLO was assumed as rigid for convenience of comparison of the numerical results with closed-form solutions for maximum accelerations predicted by the classical von Karman and Wagner. In order to emphasize the importance of the analytical estimates, the accelerations obtained analytically were plotted against the drop height for the WLO model (using the original radius of the WLO). In order to achieve accelerations comparable to the closed-form solutions, the analytical results show that, for the design of a WLO, the Wagner approach provides a reasonably correct estimate of the equivalent radius of the WLO.

Concluding Remarks

A preliminary study of simulating the water landing of a conceptual water-landing object with an explicit numerical code is presented. The nonlinear transient dynamic code with its finite-element ALE and SPH capability for analyzing large deformation structural and fluid dynamic applications is used to model the scaled down experiments. The present work is the first of its kind in testing a scaled-down model of WLO impacting ocean waters for the Indian Space Mission. An important aspect in evaluating the predictive capability of the FE-ALE and SPH is the accuracy and reliability of the numerical simulation results in determining the impact accelerations.

A constrained Lagrange interface/contact is shown to successfully capture impact phenomenon between the object and the water target. The effects of varying the vertical velocity, entry angle and the WLO weight are identified and the numerical predictions are first validated with experimental data for maximum impact accelerations. The maximum acceleration upon impact is about 5.5 g for a 0 deg pitch angle (vertical velocity tests) and 4.5 g for a 15 deg pitch test (pitch tests). Analyses were performed for the rigid object entering the water with different weights. The weight of 3.5 kg corresponds to the experimental case-II involving an electromagnetic drop mechanism. The general trend shows advantage gained in reduced g-force for a large increase in weight (3.8 g for case-II compared to 5.5 g for case-I). This indicates that the analyses performed can produce satisfactory results to use in design studies.

An important feature in simulating contact and impact problems is proper modeling of the two-phase flow with the actual modeling of the air with associated density and state equation. Previous studies in simulations of impact events in the absence of air domain resulted in very high impact accelerations with a very high frequency content, which requires filtering when compared to experimental results. In addition to the modeling of the actual air domain, another important aspect that is usually ignored in simulating such complex FSI impact event is the positioning of the rigid body with respect to the water surface. A comprehensive study using both the "realizations" facilitates the capturing of the physics of the impact event accurately and provides data sets that are comparable to experimental test cases.

Tasks performed in this study also include the comparison of the numerical solutions with analytical solutions for the rigid object and understanding the filtering techniques needed to predict the correct maximum impact accelerations. These predictions suggest that the fully coupled FSI models can capture the water-impact response accurately for all range of drop tests and there is a good comparison between the simulations and the experimental results.

Several observations can be made. Model testing is needed over a wider range of conditions to include improved tests that vary the speed, weight and entry angle and under realistic conditions existing in the oceans. Modeling of the rigid body impact problem used for correlation with the experimental results, demonstrates some of the challenging problems encountered when modeling the air and water domains.

The possibility of combining the finite element package with a computational fluid dynamics package could more accurately simulate the hydrodynamics during impact. Further levels of complexity can be introduced to the model as well as scrutinizing the results further. Future work may include more in-depth analysis of the WLO water impact pressure distribution, fully deformable vehicles and floatation studies. The development of a more accurate numerical solution to capture the nonlinear nature of the FSI problem should be pursued by employing robust modeling of the basic physics of water impact. Finally, full-scale prototype testing is needed over a wider range of conditions to include cases with varying speed, weight and entry angle under realistic conditions existing in the oceans.

Acknowledgment

References

[1] Von Karman, T., 1929, "The Impact of Seaplane Floats During Landing," NACA TN 321, National Advisory Committee for Aeronautics, Washington, DC.
[2] Wagner, H., 1932, "Trans. Phenomena Associated With Impacts and Sliding on Liquid Surfaces," J. Math. Mech., **12**(4), pp. 193–215.
[3] Miloh, T., 1991, "On the Initial-Stage Slamming of a Rigid Sphere in a Vertical Water Entry," Appl. Ocean Res., **13**(1), pp. 43–48.
[4] Brooks, J. R., and Anderson, L. A., 1994, "Dynamics of a Space Module Impacting Water," J. Spacecr. Rockets, **31**(3), pp. 509–515.
[5] Zhao, R., Faltinsen, O. M., and Aarsnes, J. V., 1996, "Water Entry of Arbitrary Two-Dimensional Sections With and Without Flow Separation," Proceedings of the 21st Symposium on Naval Hydrodynamics, National Academy Press, Washington, DC, pp. 408–423.
[6] Faltinsen, O. M., 1999, "Water Entry of a Wedge by Hydroelastic Orthotropic Plate Theory," J. Ship Res., **43**(3), pp. 180–193.
[7] Scolan, Y. M., and Korobkin, A. A., 2001, "Three-Dimensional Theory of Water Impact. Part 1. Inverse Wagner problem," J. Fluid Mech., **440**, pp. 293–326.
[8] Souli, M., Olovsson, L., and Do, I., 2002, "ALE and Fluid-Structure Interaction Capabilities in LS-DYNA," 7th International LS-DYNA Users Conference.
[9] Korobkin, A. A., and Scolan, Y. M., 2006, "Three-Dimensional Theory of Water Impact. Part 2. Linearized Wagner Problem," J. Fluid Mech., **549**, pp. 343–373.
[10] Tutt, B. A., and Taylor, A. P., 2004, "The Use of LS-DYNA to Simulate the Water Landing Characteristics of Space Vehicles," 8th International LS-DYNA Users Conference, Dearborn, MI, May 2–4.
[11] Melis, E. M., and Bui, K., 2002, "Characterization of Water Impact Splashdown Event of Space Shuttle Solid Rocket Booster Using LS-DYNA," 7th International LS-DYNA Users Conference, Dearborn, MI, May 19–21.

[12] Korobkin, A. A., 2005, "Three-Dimensional Nonlinear Theory of Water Impact," 18th International Congress of Mechanical Engineering (COBEM), Ouro Preto, Minas Gerais, Brazil.

[13] Seddon, C. M., and Moatamedi, M., 2006, "Review of Water Entry With Applications to Aerospace Structures," Int. J. Impact Eng., **32**, pp. 1045–1067.

[14] Wang, J. T., and Lyle, K. H., 2007, "Simulating Space Capsule Water Landing With Explicit Finite Element Method," 48th AIAA/ASME Conference, Waikiki, HI, pp. 23–26.

[15] Jackson, K. E., and Fuchs, Y. T., 2008, "Comparison of ALE and SPH Simulations of Vertical Drop Tests of a Composite Fuselage Section Into Water," 10th International LS-DYNA Users Conference, Dearborn, MI, June 8–10.

[16] Vandamme, J., Zou, Q., and Reeve, D. E., 2011, "Modeling Floating Object Entry and Exit Using Smoothed Particle Hydrodynamics," J. Waterw., Port, Coastal, Ocean Eng., **137**(5), pp. 213–224.

[17] Challa, R., Yim, S. C., Idichandy, V. G., and Vendhan, C. P., 2014, "Rigid-Body Water-Surface Impact Dynamics: Experiment and Semi-Analytical Approximation," ASME J. Offshore Mech. Arctic Eng., **136**, p. 011102.

[18] Scolan, Y. M., and Korobkin, A. A., 2012, "Hydrodynamic Impact (Wagner) Problem and Galin's Theorem," 27th International Workshop on Water Waves and Floating Bodies, Copenhagen, Denmark.

[19] Belytschko, T., Flanagran, D. F., and Kennedy, J. M., 1982, "Finite Element Method With User-Controlled Meshes for Fluid-Structure Interactions," J. Comput. Methods Appl. Mech. Eng., **33**, pp. 689–723.

[20] Hallquist, J. O., 1998, "LS-DYNA Theoretical Manual," Livermore Software Technology Corporation.

[21] Souli, M., and Benson, D. J. 2010, *Arbitrary Lagrangian-Eulerian and Fluid-Structure Interaction Numerical*," Wiley Publications, New York.

[22] Dalrymple, R. A., and Rogers, B. D., 2006, "Numerical Modeling of Water Waves With the SPH Method," Coastal Eng. J., **53**(2–3), pp. 141–147.

[23] Faltinsen, O. M., 2005, *Hydrodynamics of High-Speed Marine Vehicles*, Cambridge University, New York.

[24] Hirano, Y., and Miura, K., 1970, "Water Impact Accelerations of Axially Symmetric Bodies," J. Spacecr. Rockets, **7**(6), pp. 762–764.

[25] Gingold, R. A., and Monaghan, J. J., 1977, "Smoothed Particle Hydrodynamics: Theory and Application to Nonspherical Stars," Mon. Not. R. Astron. Soc., **181**, pp. 375–389.

[26] Lucy, L., 1977, "A Numerical Approach to Testing of the Fusion Process," Astron. J., **88**, pp. 1013–1024.

[27] Herault, A., Vicari, A., Negro, C., and Dalrymple, R. A., 2009, "Modeling Water Waves in the Surf Zone With GPU-SPHysics," 4th International SPHERIC Workshop, Nantes, France, pp. 27–29.